Katsumata *et al. Earth, Planets and Space* (2021) 73:72
https://doi.org/10.1186/s40623-021-01391-7

Earth, Planets and Space

FULL PAPER Open Access

Rapid estimation of tsunami earthquake magnitudes at local distance

Akio Katsumata*, Masayuki Tanaka and Takahito Nishimiya

Abstract

A tsunami earthquake is an earthquake event that generates abnormally high tsunami waves considering the amplitude of the seismic waves. These abnormally high waves relative to the seismic wave amplitude are related to the longer rupture duration of such earthquakes compared with typical events. Rapid magnitude estimation is essential for the timely issuance of effective tsunami warnings for tsunami earthquakes. For local events, event magnitude estimated from the observed displacement amplitudes of the seismic waves, which can be obtained before estimation of the seismic moment, is often used for the first tsunami warning. However, because the observed displacement amplitude is approximately proportional to the moment rate, conventional magnitudes of tsunami earthquakes estimated based on the seismic wave amplitude tend to underestimate the event size. To overcome this problem, we investigated several methods of magnitude estimation, including magnitudes based on long-period displacement, integrated displacement, and multiband amplitude distribution. We tested the methods using synthetic waveforms calculated from finite fault models of tsunami earthquakes. We found that methods based on observed amplitudes could not estimate magnitude properly, but the method based on the multiband amplitude distribution gave values close to the moment magnitude for many tsunami earthquakes. In this method, peak amplitudes of bandpass filtered waveforms are compared with those of synthetic records for an assumed source duration and fault mechanism. We applied the multiband amplitude distribution method to the records of events that occurred around the Japanese Islands and to those of tsunami earthquakes, and confirmed that this method could be used to estimate event magnitudes close to the moment magnitudes.

Keywords: Tsunami earthquake, Magnitude, Velocity-type strong-motion seismometer, Tsunami warning

Introduction

Some earthquakes generate large tsunamis even though their surface wave magnitudes are relatively small (Kanamori 1972). Such earthquakes, which have abnormally long rupture durations, are called tsunami earthquakes. The 1896 Meiji-Sanriku earthquake off northeast Japan (Kanamori 1972; Tanioka and Satake 1996), the 1946 Aleutian Island earthquake (Kanamori 1972; Johnson and Satake 1997), the 1992 Nicaragua earthquake (M_S 7.2, M_w 7.6, source duration ~100 s) (Kanamori and Kikuchi 1993; Satake 1994; Polet Kanamori 2000), the 1994 Java earthquake (M_S 7.2, M_w 7.8, source duration 80–90 s) (Polet Kanamori 2000; Abercrombie et al. 2001; Polet and Thio 2003), the 1996 Peru earthquake (M_S 6.6, M_w 7.5, source duration 50 s) (Heinrich et al. 1998; Ihmlé et al. 1998), the 2006 Java earthquake (M_S 7.7, M_w 7.7, source duration 185 s) (Ammon et al. 2006; Fan et al. 2017), and the 2010 Mentawai earthquake (M_S 7.8, M_w 7.8, source duration 90–125 s) (Newman et al. 2011; Lay et al. 2011) were all tsunami earthquakes. The moment magnitudes M_w (Kanamori 1977) given here for these events are based on global CMT solutions (Dziewonski et al. 1981; G Ekström et al. 2012). These tsunami earthquakes occurred at shallow interplate boundaries near trench axes, and their slow rupture speeds are considered to relate to the frictional properties around shallow plate boundaries (e.g., Polet Kanamori 2000; Bilek and Lay 2002).

*Correspondence: akatsuma@mri-jma.go.jp
Department of Seismology and Tsunami Research, Meteorological Research Institute, 1-1 Nagamine, Tsukuba, Ibaraki 305-0052, Japan

Springer Open

© The Author(s) 2021. This article is licensed under a Creative Commons Attribution 4.0 International License, which permits use, sharing, adaptation, distribution and reproduction in any medium or format, as long as you give appropriate credit to the original author(s) and the source, provide a link to the Creative Commons licence, and indicate if changes were made. The images or other third party material in this article are included in the article's Creative Commons licence, unless indicated otherwise in a credit line to the material. If material is not included in the article's Creative Commons licence and your intended use is not permitted by statutory regulation or exceeds the permitted use, you will need to obtain permission directly from the copyright holder. To view a copy of this licence, visit http://creativecommons.org/licenses/by/4.0/.

Submarine landslides caused by strong ground motions produced by large earthquakes have also caused disastrous tsunamis (Okal and Synolakis 2004). Those earthquakes, although accompanied by high large tsunamis, also have relatively small seismic amplitude. Here, we consider only earthquakes with long source durations.

For tsunami warning purposes, rapid estimation of event magnitude soon after event detection is essential, because the seismic moment of tsunami earthquakes can be used to estimate the height of the expected tsunami. At present, seismic moment can be estimated within 10 min of event detection by W-phase analysis of regional seismic network data (Kanamori and Rivera 2008; Usui and Yamauchi 2013). However, tsunamis generated by large local events can arrive at the shoreline in less than 10 min. The Japan Meteorological Agency uses a magnitude determination method based on maximum ground displacements (Katsumata 2004) along with a few additional methods (Japan Meteorological Agency 2013; Katsumata et al. 2013) for huge earthquakes so that the first tsunami warning can be issued within about 3 min of event detection. Because far-field displacement is proportional to the seismic moment rate (e.g., Aki and Richards 2002), the longer the duration of an event, the smaller the displacement amplitude becomes. As a result, estimated magnitudes of tsunami earthquakes based on maximum ground displacement are underestimated. To overcome this problem, Tsuboi et al. (1995) proposed using the *P*-wave moment magnitude M_{wp}, which is obtained by integrating broadband seismometer records of *P*-waves, to estimate moment magnitude. They considered the amplitude of the second-order integral of broadband data to be proportional to seismic moment. However, application of the M_{wp} method to the 1992 Nicaragua earthquake yielded an estimated magnitude of less than 7.0 (Tsuboi et al. 1995). Hara (2007) used a magnitude determination method based on the duration of high-frequency energy radiation and the maximum *P*-wave displacement amplitude and obtained values consistent with moment magnitudes, even for tsunami earthquakes. Kawamoto et al. (2017) developed the REGARD fault parameter estimation method based on real-time GNSS data for tsunami-warning purposes. The REGARD method should yield appropriate magnitudes even for tsunami earthquakes, but a tsunami earthquake with an epicenter near the Japan trench, such as the 1896 Sanriku earthquake, might not cause enough crustal deformation for analysis by real-time GNSS. For example, the crustal deformation of the shoreline given the fault model (strike 190°, dip 20°, rake 90°, length 210 km, width 50 km, seismic moment 12×10^{20} Nm; Tanioka and Satake 1996) of the 1896 Sanriku earthquake, calculated by the method of Okada (1992) using a rigidity of 6.3×10^{10} N/m^2, was several centimeters, a little smaller than the REGARD threshold (10 cm). For this calculation, we used this rigidity value, which is larger than that indicated by Tanioka and Satake (1996) because crustal deformation was evaluated at a point distant from the fault.

In this study, we investigated several magnitude estimation methods for tsunami earthquakes, based on the long-period displacement, integrated displacement, and multiband amplitude distribution recorded at local distance from the earthquake epicenter by velocity-type strong-motion (VSM) and broadband (BB) seismometers, to use for first tsunami warnings. The *P*, *S*, and surface wave seismic phases from long-duration earthquakes overlap when they arrive at a near-field station. Magnitude can be estimated at local distance more quickly by using mixed phases than by using only *P*-waves (Katsumata et al. 2013). We therefore developed magnitude estimation methods based on the amplitudes of mixed phases. Then we evaluated the methods by using finite fault models and data obtained around the Japanese Islands and other regions.

Data

We used data obtained by VSM and BB seismometers operated by the National Research Institute for Earth Science and Disaster Resilience (NIED) for events around the Japanese Islands (Fukuyama et al. 1996). A VSM seismometer has a similar frequency response to a BB seismometer but covers a higher amplitude range. For the tsunami earthquakes, we used data archived by the Incorporated Research Institutions for Seismology.

Real-time processing is required for our magnitude estimation methods, so time-domain processing with a recursive filter is necessary. Instrumental responses were corrected by using recursive digital filters similar to Zhu (2003) and Kanamori and Rivera (2008). If the response $H(s)$ in the Laplace transform expression of the VMS and BB seismometers on the long period side is given by two conjugate or two real poles (s_{L1} and s_{L2}), then

$$H(s) = \frac{s^2}{(s - s_{L1})(s - s_{L2})}. \tag{1}$$

For the values of the poles, we used those given by National Research Institute for Earth Science and Disaster Resilience (2019). The recursive filter is obtained by calculating the *z*-transform of the inverse of Eq. 1.

$$\begin{aligned} H^{-1}(z) =& \{(1 - cs_{L1} - cs_{L2} + c^2 s_{L1} s_{L2}) + (-2 + 2c^2 s_{L1} s_{L2}) z^{-1} \\ &+ (1 + cs_{L1} + cs_{L2} + c^2 S_{L1} S_{L2}) z^{-2}\} / (1 - 2z^{-1} + z^{-2}), \end{aligned} \tag{2}$$

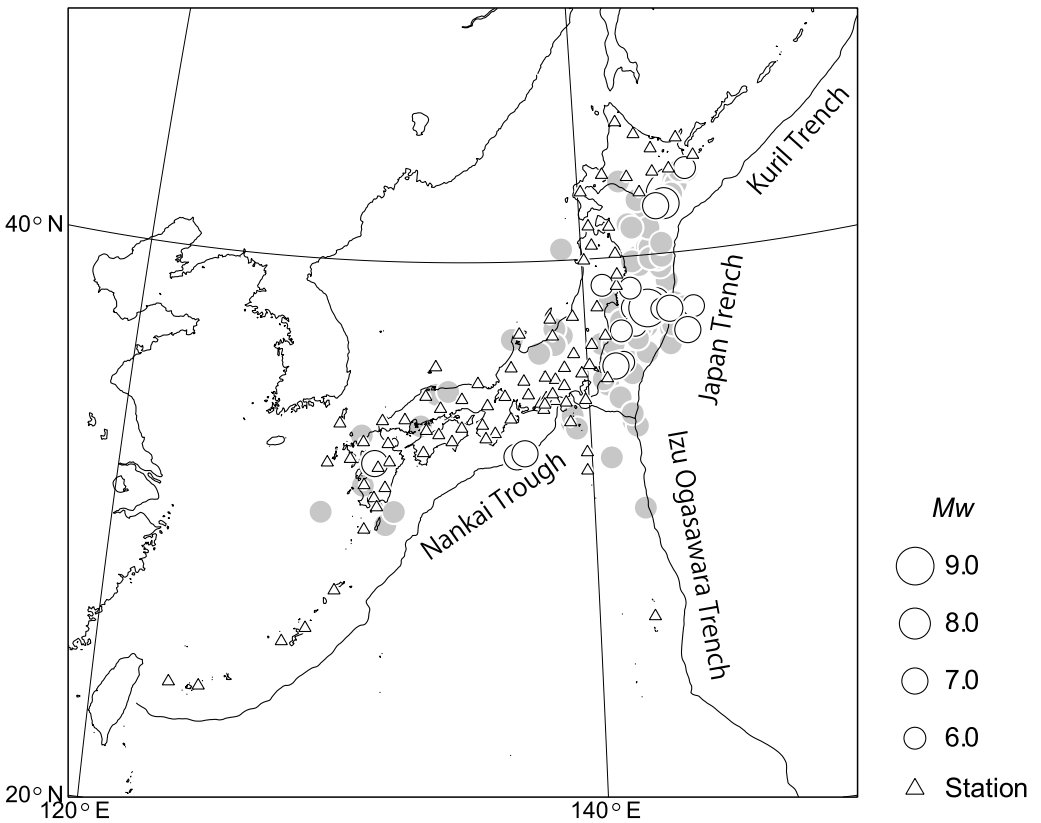

Fig. 1 Map showing the locations of the stations (triangles) and epicenters (open circles) of the earthquakes used to obtain the regression relationship between earthquake magnitude and observed peak amplitudes. Open and gray-filled circles denote the events used for Figs. 5 and 7

where $c = \Delta t/2$ and Δt is the sampling interval. When the response on the long period side is given by a single real pole (s_L), the recursive filter is

$$H^{-1}(z) = \frac{(1 - cs_L) + (-1 - cs_L)z^{-1}}{1 - z^{-1}}. \quad (3)$$

Empirical method based on observed amplitude

We derived empirical formulas to represent the relationships between moment magnitude and observed peak amplitudes using data from ordinary events around the Japanese Islands. We examined three types of amplitudes: highpass-filtered displacement (cutoff period 200 s), highpass-filtered integrated displacement (cutoff period 200 s), and bandpass-filtered displacement (passband 200–400 s). We expected integrated displacement would reflect seismic moment rather than moment rate (Tsuboi et al. 1995), and that long period displacement would be relatively insensitive to source duration. As a target, we assumed an earthquake with a rupture duration of 100 s. We set the cutoff period for the highpass-filtered displacement and the highpass-filtered integrated displacement to 200 s, twice the assumed rupture duration. A fourth-order Bessel high-pass filter (Katsumata 1993) was applied to the displacement to suppress the baseline shift of the seismic wave caused by the three time integrations (two for the instrumental response correction by Eq. 2 and one for the conversion from velocity to displacement) during continuous filtering in a real-time system. A fifth-order Bessel high-pass filter was applied to the integrated displacement.

For this analysis, we selected events that occurred near the main islands of Japan (open circles in Fig. 1, Table S1), based on hypocenter locations in the Seismological Bulletin of Japan (Japan Meteorological Agency 2019), to avoid the effect of small amplitudes attributable to the radiation pattern. Although large earthquakes have occurred around the Kuril Islands, stations on the Japanese Islands are located approximately along the null axis of the seismic wave radiation pattern from those earthquakes. We set a threshold of $M_w > 6.8$ as an approximate magnitude threshold of hazardous tsunami potential. Whereas these events were not tsunami earthquakes, we expected empirical analyses on the integrated displacement and long-period displacement of these events would provide formulas reflecting their seismic moments rather then their moment rates.

For example, Fig. 2 shows an original seismogram recorded at Urahoro station (URH, epicentral distance 132 km) during the 2003 Tokachi-oki earthquake (25 September UTC, M_w 8.3), together with the displacement and the integrated displacement records obtained after instrumental response correction and integration.

It is possible that some amplitude data were contaminated with instrumental noise, and it is necessary to exclude those data for proper magnitude estimation. For example, Fig. 3 shows peak integrated displacement amplitudes and travel times for an earthquake (M_w 6.4) that occurred on 24 January 2018 east off northeast Japan. Here, T_0 is the origin time, T_P and T_S are the calculated *P*- and *S*-wave travel times (Ueno et al. 2002), and T_D is the assumed rupture duration ($2 \times 10^{(M_w-5)/2}$ s). The data from BB seismometers are distributed between $T_0 + T_S$ (solid red line in Fig. 3) and $T_0 + 2.5T_S + T_D$ (dashed red line), whereas the data from VSM seismometers are distributed mainly after $T_0 + 2.5T_S + T_D$. The data after $T_0 + 2.5T_S + T_D$ are considered to be contaminated by instrumental noise because of the scattered travel times and because the amplitudes are larger than the BB seismometer amplitudes. We divided peak amplitude data for 366 events into "Good" and "Not Good" data, where peak amplitudes between $T_0 + T_S$ and $T_0 + 2.5T_S + T_D$ were considered to be Good data, and plotted the data against the peak digital counts (BIT; Fig. 4, left panels) and the integrated displacement amplitudes (right side). The result shows that data with large integrated displacement amplitudes may not be reliable, but the digital count of the original data can be used as an index for distinguishing reliable from unreliable data. In

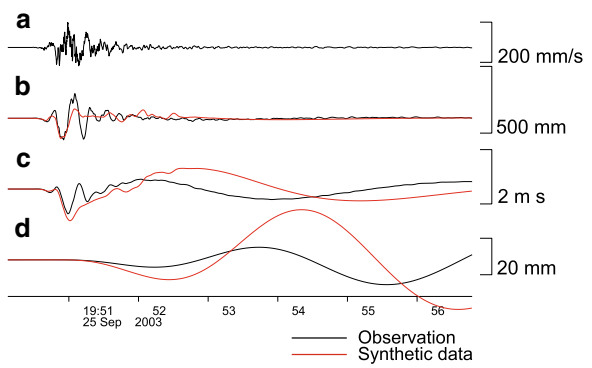

Fig. 2 Example seismic waveforms. **a** Original seismogram of the 2003 Tokachi-oki earthquake recorded at Urahoro station with a velocity-type strong-motion seismometer. **b** Displacement record (black curve) obtained after instrumental correction and integration of the original record shown in **a**. **c** Integrated displacement record (black curve) obtained from the original record shown in **a**. (d) Bandpass (200–400 s) filtered displacement record (black curve) obtained from the original record shown in **a**. The red curves in **b**–**d** show synthetic records for the finite fault model of U. S. Geological Survey (2020)

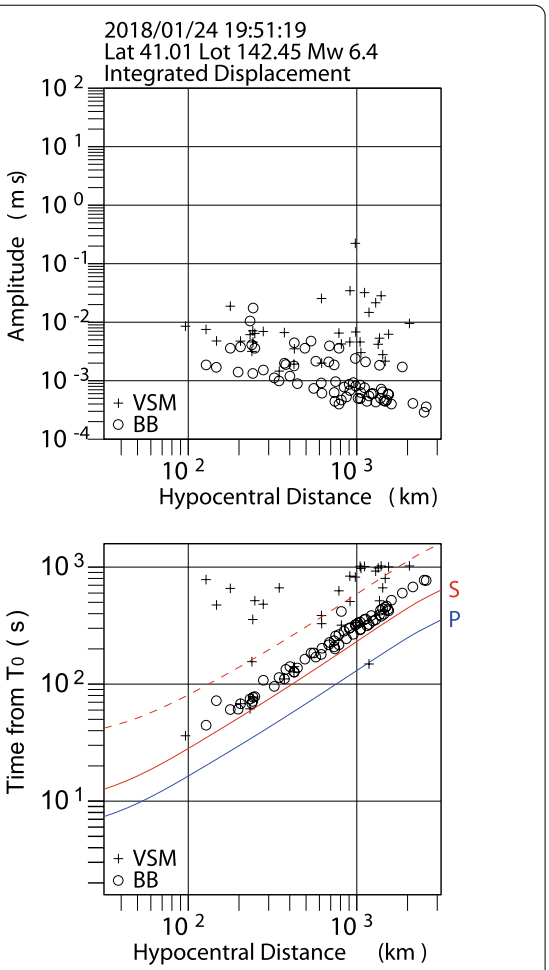

Fig. 3 Peak amplitudes of integrated displacement (upper) for an earthquake that occurred on 24 January 2018 (M_w 6.4), and travel times to peak amplitude (lower) in relation to hypocentral distance for amplitudes observed with velocity-type strong-motion (VSM) seismometers (crosses) and broadband (BB) seismometers (circles). The solid blue, solid red, and dashed red curves show the calculated values of $T_0 + T_P$, $T_0 + T_S$, and $T_0 + 2.5T_S + T_D$, respectively, where T_0 is origin time, T_P is *P*-wave travel time, T_S is *S*-wave travel time, and T_D is the assumed source duration. The travel times were calculated by using the velocity structure of Ueno et al. (2002)

Table 1 Velocity structure model used to calculate the synthetic records

Depth(top) km	Velocity (*P*) km/s	Velocity (*S*) km/s	Density g/cm^3	Q_P	Q_S
0.0	4.2	2.42	2.4	200	100
2.4	5.3	3.06	2.6	300	150
4.0	6.1	3.52	2.7	300	150
14.6	6.7	3.87	3.0	500	250
31.5	8.0	4.62	3.2	600	300

Table 2 Magnitude estimation for finite fault models (U. S. Geological Survey 2020) of tsunami earthquakes and two major earthquakes around Japan. The moment magnitude M_W, magnitudes based on highpass-filtered displacement (cutoff period 200 s) (M_{D200}), highpass-filtered integrated displacement (cutoff period 200 s) (M_{ID200}), bandpass-filtered displacement (passband 200–400 s) ($M_{D200-400}$), and multiband amplitude distribution (M_{BA}) are compared

	M_W	M_{D200}	M_{ID200}	$M_{D200-400}$	M_{BA}
1992 Nicaragua	7.6	6.7	6.9	7.2	7.5
1994 Java	7.8	7.5	7.5	7.2	7.6
1996 Peru	7.5	7.4	7.2	7.2	7.4
2006 Java	7.7	6.9	6.9	7.2	7.3
2010 Mentawai	7.8	7.3	7.2	7.3	7.5
2003 Tokachi	8.3	8.4	8.2	7.9	8.1
2011 Tohoku	9.1	8.9	8.8	8.9	8.9

our analysis, therefore, we used amplitude data with time t, where $T_0 + T_S < t < T_0 + 2.5T_S + T_D$, and original digital data amplitudes $> 2^{10}$. Because duration cannot be set appropriately before the magnitude is estimated, we assumed T_D to be constant at 200 s.

Using the peak amplitude (A) of the vertical component, we obtained the following empirical relationship:

$$M_w \simeq a \log_{10} A + b \log_{10} R + c, \tag{4}$$

where a, b, and c are constants; M_w is the moment magnitude calculated with global CMT data (Dziewonski et al. 1981; G Ekström et al. 2012); and R is hypocentral distance (≤1000 km). We selected the vertical component because we expected dip slip on the fault to result in a large vertical displacement amplitude and because the vertical component would be relatively insensitive to the inclination of the crustal deformation.

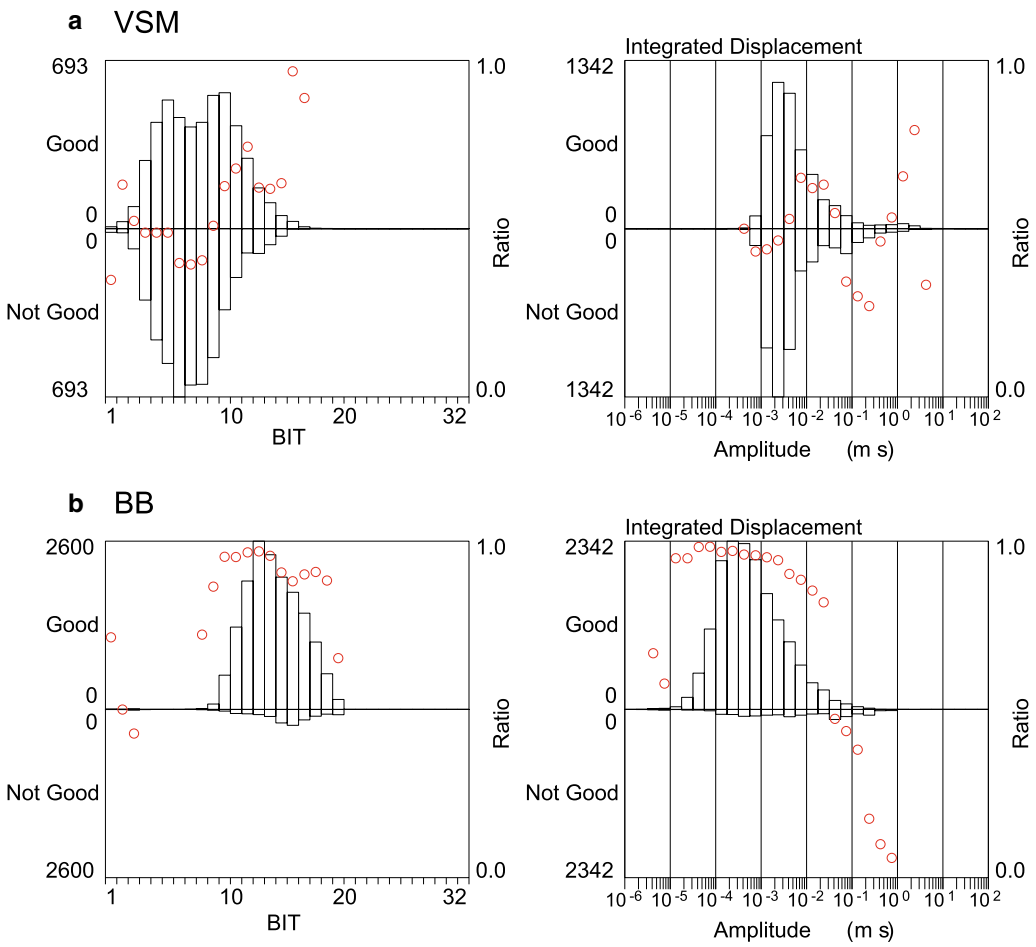

Fig. 4 Distinguishing "Good" and "Not Good" data. Good data are data with peak integrated displacement times between $T_0 + T_S$ and $T_0 + 2.5T_S + T_D$, as shown in Fig. 3. The peak digital counts of the original record (BIT, left) and the integrated displacement amplitudes (right) are compared between **a** velocity-type strong-motion (VSM) seismometers and **b** broadband (BB) seismometers. Good data are shown above the 0 line, and Not Good data (as defined in the text) are shown below the line. Ratios of Good good to the total number of data are shown by red circles (right-side scale)

We expected b in Eq. 4 to be insensitive to earthquake size. By averaging the regression line slopes of 20 events (open circles in Fig. 1, Table S1), including inland events, with $M_w > 6.8$, we obtained values of $b_{D200} = 1.10$ for highpass-filtered displacements with a 200 s cutoff, $b_{ID200} = 0.857$ for highpass-filtered integrated displacements with a 200 s cutoff, and $b_{D200-400} = 0.923$ for bandpass-filtered displacement with a passband of 200-400 s. a and c were obtained by minimizing the expression $\Sigma_i\{M_{wi} - (a\log_{10}A + b\log_{10}R + c)_i\}^2$, where i is an index of events. The resulting magnitude estimation formulas for the three types of amplitudes are

$$M_{D200} = 1.06\log_{10}A_{D200} + 1.10\log_{10}R + 6.69, \quad (5)$$

$$M_{ID200} = 0.919\log_{10}A_{ID200} + 0.857\log_{10}R + 6.31, \quad (6)$$

$$M_{D200-400} = 0.813\log_{10}A_{D200-400} + 0.923\log_{10}R + 7.63. \quad (7)$$

We compared M_{D200}, M_{ID200}, and $M_{D200-400}$ obtained with Eqs. 5–7 with M_w (Fig. 5). We included smaller events ($M_w > 6.0$) for this figure to check the results for smaller events. Underestimation is recognized for events of $M_w \sim 6.0$ in all three methods. For quick magnitude estimation, it is necessary to limit the number of stations used. Therefor, magnitudes estimated with data from the 10 closest stations (crosses in Fig. 5) are shown together with those estimated by using all available data (circles). For events with $M_w > 6.8$, the root mean squares of $M_{D200} - M_w$, $M_{ID200} - M_w$, and $M_{D200-400} - M_w$ for magnitudes estimated by using all data within 1000 km were 0.18, 0.14, and 0.15, respectively.

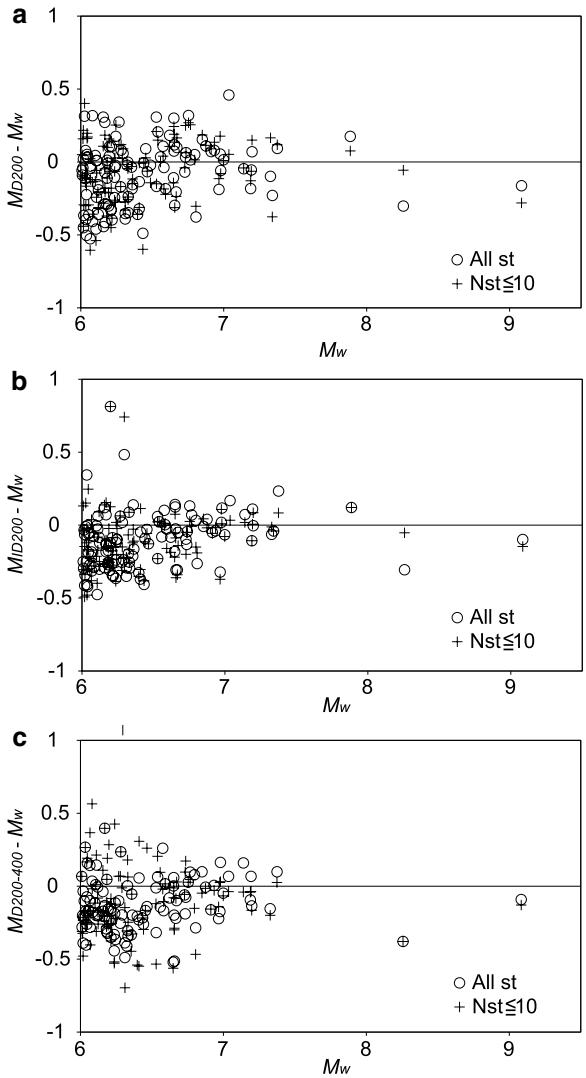

Fig. 5 Comparison of various estimated magnitudes with the moment magnitude (M_w). **a** Comparison between the magnitude based on highpass-filtered (200 s cutoff) displacement (M_{D200}) and M_w. **b** Comparison between the magnitude based on integrated displacement (200 s cutoff, M_{ID200}) and M_w. **c** Comparison between the magnitude based on bandpass-filtered (200–400 s) displacement ($M_{D200--400}$) and M_w

Magnitude based on multiband amplitude distribution (M_{BA})

Rupture duration is a key factor used to characterize a tsunami earthquake. To estimate the characteristic duration of an earthquake, we examined the multiband amplitude distribution obtained from the peak amplitudes of bandpass-filtered seismic records with passbands at intervals of $10^{0.2}$ from 2.51 to 631 s. The ratio of upper and lower limits of passband intervals was set to $10^{0.6}$ so that the passbands overlapped with each other. In this case, the amplitudes of 10 bands were used. To exclude noise-contaminated data, the same peak digital count limitation (described in the previous section) was applied in this analysis. Overlapping passbands were used to capture relatively short-duration seismic wave increases. If the period on the shorter side of a passband is long enough, it takes a long time for the seismic wave to reach its peak, and this long time could become a problem for rapid magnitude estimation. We compared the amplitude distributions between bandpass-filtered observed and synthetic records by assuming various rupture durations. As an example, multiband amplitude distributions of the 2003 Tokachi-oki earthquake (M_w8.3) are shown in Fig. 6. The black and red bars show peak amplitudes of bandpass-filtered observed and synthetic records. The synthetic records were calculated by assuming a seismic moment value, M_{0_A}, and various source durations. The durations were set at $10^{0.1}$ intervals from 2.5 to 398 s. Each graph in Fig. 6 compares the observed amplitude

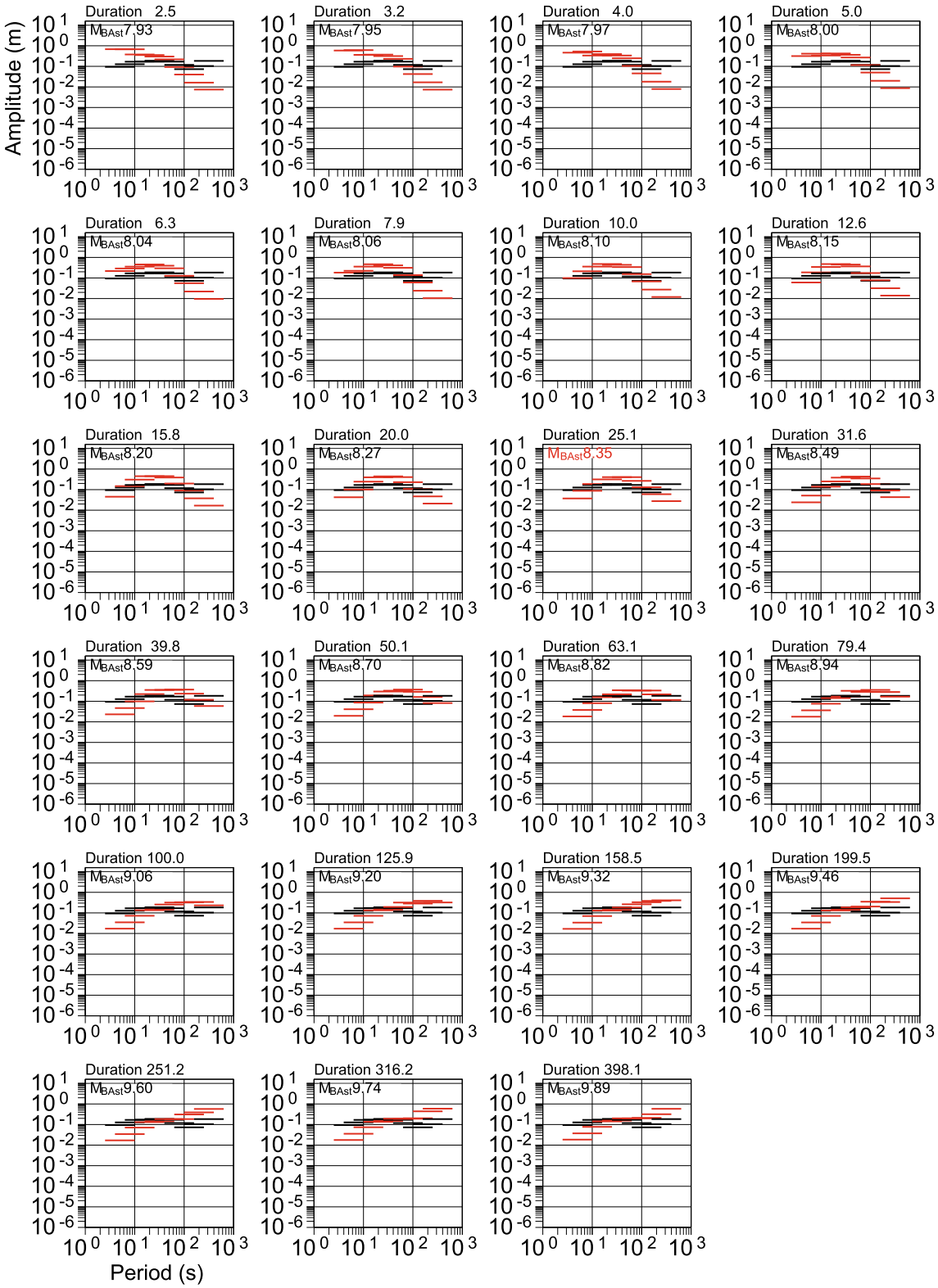

Fig. 6 Examples of multiband amplitude distributions of the 2003 Tokachi-oki earthquake in relation to seismic wave period. The black bars indicate observed peak displacements of the bandpass-filtered seismic record, and the red bars indicate those of the synthetic records fitted to the observation. The length of each bar shows the passband range. Each graph shows comparison for an assumed source duration. The estimate magnitude for each duration is indicated at the upper left of the graph. Duration of 25 s showed the best fit in this case

distribution with the synthetic one for a specific source duration. The best source duration was selected based on the standard deviation of the least squares fitting, which was 25 s in the case of Fig. 6. The earthquake magnitude for a station, M_{BAst}, was estimated from the assumed seismic moment for the synthetic records and logarithmic average difference between observed and synthetic amplitudes, $\overline{\log_{10} A_{oi} - \log_{10} A_{si}}$, for the selected source duration as

$$M_{0st} = M_{0_A} + 10^{\overline{\log_{10} A_{oi} - \log_{10} A_{si}}},$$
$$M_{BAst} = (\log_{10} M_{0st} - 9.1)/1.5,$$

where M_{0st} is estimated seismic moment for a station, A_{oi} and A_{si} are the observed and synthetic peak amplitudes of the selected source duration for the ith bandpass filter.

For data from multiple stations, the average was calculated over station magnitudes, M_{BAst}, using the duration estimated to be the mode. The minimum number of data to estimate M_{BA} was set at three so that extraordinary data would be rejected. If a dominant duration was not found, sum over three durations was evaluated to determine the dominant duration. The number of stations was limited to 10 to reduce the estimation time, because the results for 10 stations were almost the same as those for 20 stations.

The synthetic records were calculated by the method of Takeo (1985) for a point source at the hypocenter with the velocity structure shown in Table 1. Fault parameters must be assumed to calculate synthetic records. The strike and dip were assumed from the subducting plate geometry. The rake was set at 90° by assuming a pure dip slip. The assumed source time function was $\{1 - \cos(\pi t/D)\}/2$, where t and D denote time and source duration, respectively. Synthetic records to be used for rapid estimation soon after an earthquake occurrence were obtained from Green's functions calculated in advance. We prepared Green's functions for six seismic moment components at 2 km intervals up to 1,000 km in epicentral distance and at 2 km intervals down to 100 km depth.

We compared M_w with the magnitude estimated by observed data using the multiband amplitude distribution for events around the Japanese Islands (Fig. 7). For events with $M_w > 6.8$, the root mean square of $M_{BA} - M_w$ was 0.14. Result for smaller events ($M_w > 6.0$) were also shown in the figure. Overestimation is recognized in Fig. 7 for events of $M_w \sim 6$. We tested the depth dependence of M_{BA} by changing the assumed focal depth from 2 km to 50 km for the 2003 Tokachi-oki earthquake; the resultant $M_{BA} - M_w$ value was within about 0.3 magnitude unit.

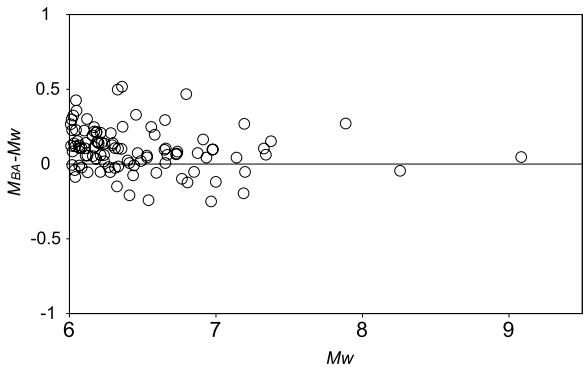

Fig. 7 Comparison of magnitudes estimated from the multiband amplitude distribution (M_{BA}) with M_w for events around Japan

Discussion

Evaluation with finite fault models

The proposed methods were tested by using finite fault models estimated by U. S. Geological Survey (2020). Because our main targets are tsunami earthquakes occurring around the Japanese Islands, we assumed that the past tsunami earthquakes occurred off Tohoku, Japan (Fig. 8), and that the seismic records were obtained by the current Japanese seismic network (Fig. 1). For each event, a synthetic record was calculated as the summation of seismic records from point sources on sub-faults (Fig. 8) by the method of Takeo (1985).

The estimated magnitudes are listed in Table 2 along with the results for the finite fault models of two major earthquakes around Japan, shown for comparison as examples of ordinary events. Magnitudes based on the three types of observed amplitudes (M_{D200}, M_{ID200}, and $M_{D200-400}$) underestimated the sizes of these tsunami earthquakes, especially those of the 1992 Nicaragua and the 2006 Java earthquakes, whereas M_{BA} values were closer to M_w for nearly all events.

All of the magnitudes based on the observed amplitudes tended to underestimate earthquake magnitudes. Figure 9 shows the relationship between peak amplitude normalized by the amplitude of the original model (U. S. Geological Survey 2020) and the rupture duration ratio calculated using the finite fault model for the 2003 Tokachi-oki earthquake. The amplitudes of displacement, integrated displacement, and bandpass-filtered displacement decreased quickly as the assumed rupture duration became longer. The synthetic records for the finite fault model (shown in Fig. 2) were obtained by convolution between the Green's function and the source time function, and averaging of the Green's function over a long rupture duration can explain the small peak amplitudes. The same cause may account for the M_{wp}

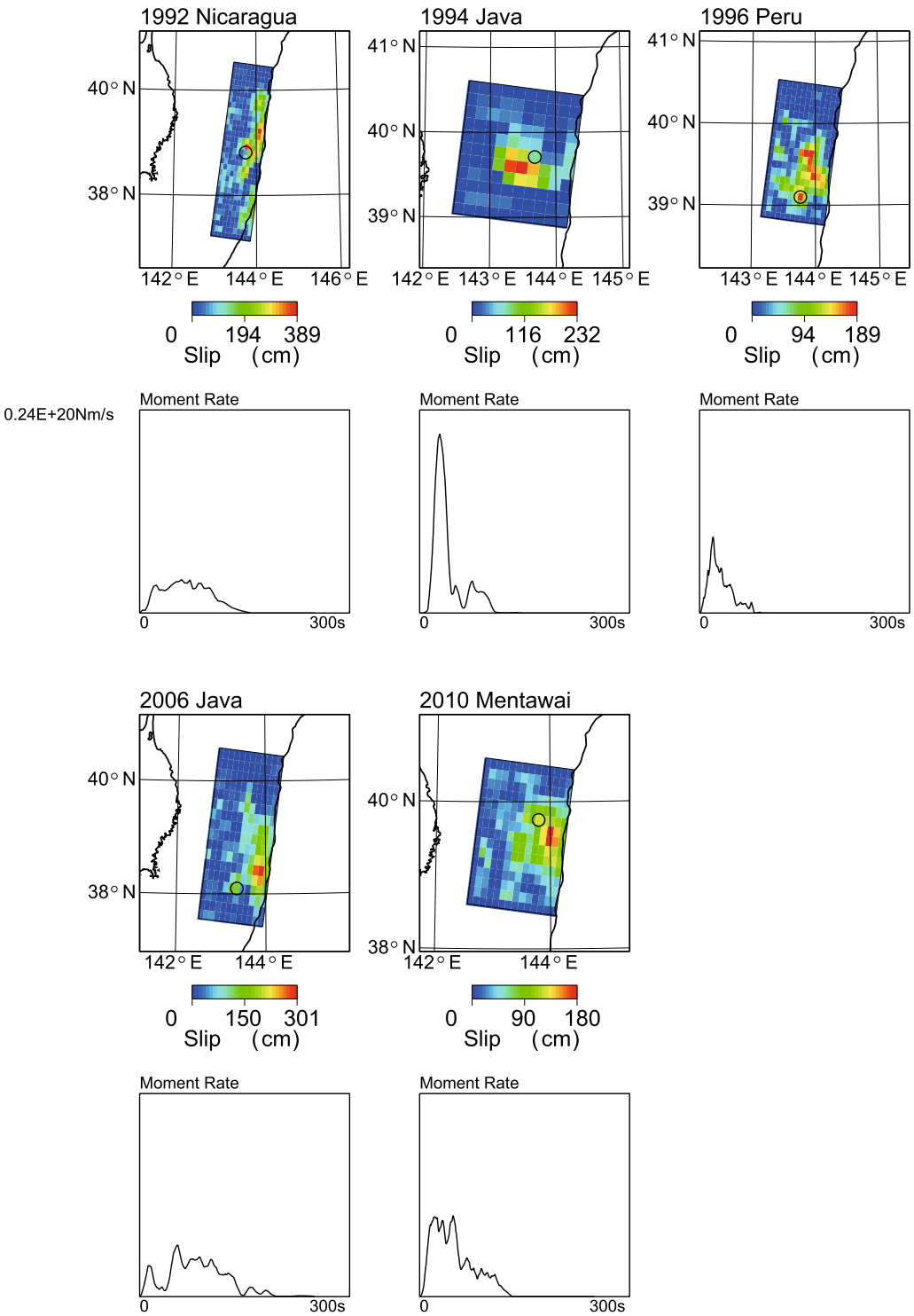

Fig. 8 (Upper) The finite fault models (U. S. Geological Survey 2020) used to test proposed magnitudes. The five tsunami earthquakes were assumed to occur off Tohoku, Japan. On each map, the circle indicates the epicenter. The various magnitudes were estimated (Table 2) for synthetic records calculated with these fault models. (Lower) Source time function of each event

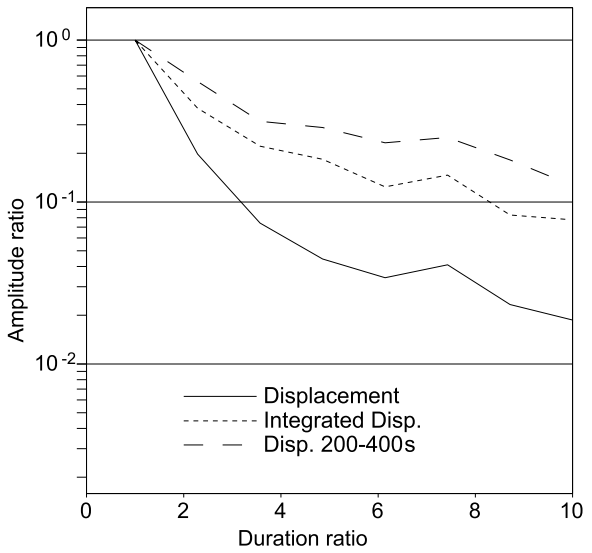

Fig. 9 Amplitude ratio of synthetic records between that for the original finite fault model (U. S. Geological Survey 2020) and that with a time-stretched source time function of $f(t/r_t)/r_t$, where t denotes time, $f(t)$ the original source time function, and r_t temporal stretching ratio (shown on the horizontal axis). The amplitude was evaluated at Urahoro station for the 2003 Tokachi-oki earthquake. Three types of amplitudes are shown, highpass filtered displacement (200-s cutoff, solid line); highpass filtered integrated displacement (200-s cutoff, dashed line); bandpass-filtered displacement (200-400 s, long-dashed line)

underestimation of the magnitude of the 1992 Nicaragua earthquake by Tsuboi et al. (1995).

Comparison of the source time functions of the tsunami earthquakes (Fig. 8) shows that the peak moment rates over the durations of the 1992 and 2006 events were relatively low compared with those of the 1994, 1996, and 2010 events; the source time functions of the 1994, 1996, and 2010 events show clear peaks, whereas those of the 1992 and 2006 events are relatively flat. These differences in the source time functions would have affected the degree to which the observed amplitude underestimated M_w (Table 2).

One way of compensating the underestimation seen in Table 2 would be a safety factor in tsunami height estimation. The average of $M_{BA} - M_w$ in Table 2 including the 2003 and 2011 events is −0.2. However, $M_{BA} - M_w$ obtained with observed data for the 2003 and 2011 events (Fig. 7) are different from those in Table 2. Because number of samples is not many and results of simulation and observation are a little different, we do not show a specific value of the safety factor for M_{BA} here. On the other hand, Tanioka and Seno (2001) discussed sediment effect for the 1896 Sanriku tsunami earthquakes. A safety factor for the sediment or low-rigidity effects should be added in practical use for the events near the trench.

Application to the observed records of the tsunami earthquake

We applied the M_{BA} magnitude estimation method to the observed records of tsunami earthquakes. However, not enough data were available for the 1992 Nicaragua, 1994 Java, 1996 Peru, and 2006 Java tsunami earthquakes. Although data were available from two seismic stations within 1000 km from the epicenter of the 2006 Java event, they were insufficient for estimating M_{BA}. For the 2010 Mentawai earthquake (M_w7.8), we obtained M_{BA}7.7, which is close to the moment magnitude of this tsunami earthquake.

A value of M_{BA} 7.5 for this earthquake was obtained from the finite fault model (Table 2) in which source location was assumed off Tohoku, Japan. We calculated synthetic records for this event with assuming its original source location and real station distribution, and a value of M_{BA} 7.5 was obtained, which was the same as that in Table 2. The reason of the underestimation in simulation seems not in the relative locations of stations.

BB seismometer networks have been enhanced after the tsunami earthquakes in Table 2. It would be possible to estimate M_{BA} for the all of the past tsunami earthquakes if they occur in the future. Because availability of VSM data is not enough except for in Japan, data records in the areas close to sources would be partly clipped for large earthquakes. Although data of a few stations were off the scale in the case of the 2010 Mentawai earthquake, it was possible to estimate M_{BA} with the remaining data for the earthquake.

Effect on tsunami height estimation from magnitude underestimation

Table 2 suggested underestimation of M_{BA} for an event similar to the 2006 Java earthquake. We calculated tsunami heights for the model of the event (M_w 7.7) shown in Fig. 8 and that with reduced magnitude (M_w 7.3) with JAGURS tsunami simulation code (Baba et al. 2017) and bathymetry data by Disaster Management Council of Japan (2003). Nonlinear longwave equation code in JAGURS and nested grids of intervals 1,350 m, 450 m, and 150 m were used for the tsunami simulation. Crustal deformation was calculated by the method of Okada (1992). A rigidity of 30 GPa was assumed for the crustal deformation calculation and calculating fault slip from seismic moment. The calculated tsunami heights along water depth of 100 m are shown in Fig. 10. The tsunami height difference was 3.6–7.5 times between the M_w 7.7 and M_w 7.3 models, which reflected the corresponding seismic moment difference. Figure 10 indicates that a possibility of serious underestimation could occur in

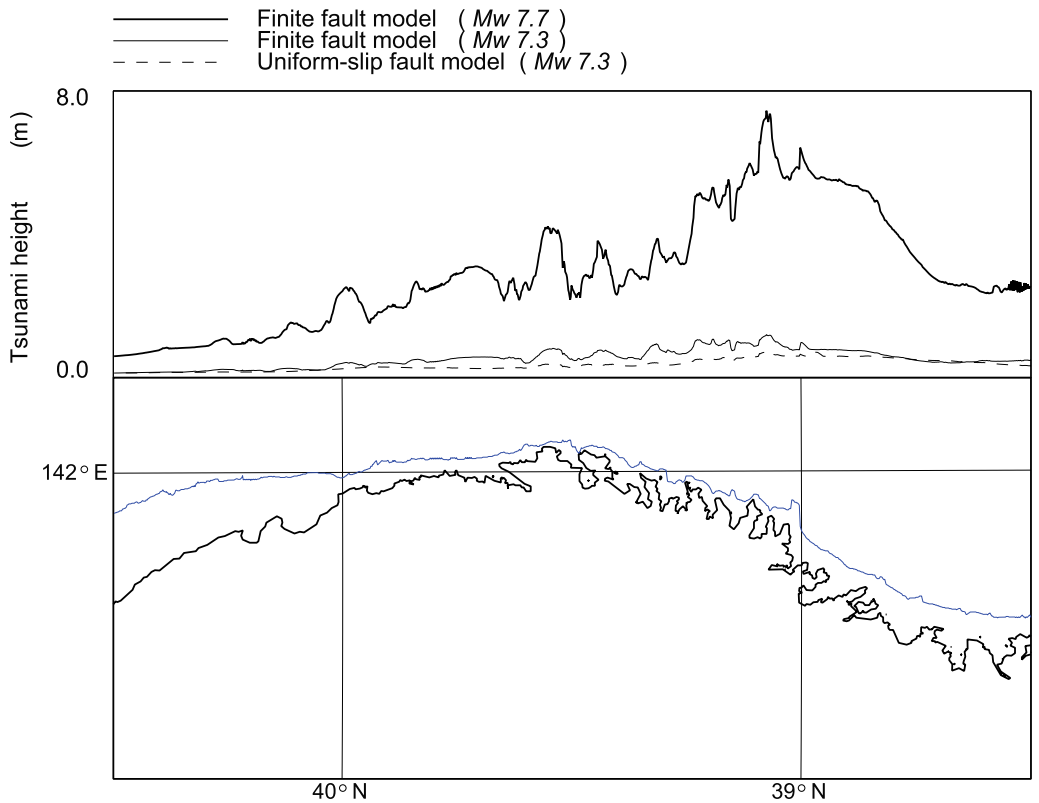

Fig. 10 Comparison of tsunami heights calculated for the finite fault model of the 2006 Java earthquake (M_w 7.7, Fig. 8, the thick solid curve), that of reduced magnitude (M_w 7.3, the thin solid curve), and a uniform-slip fault model (M_w 7.3, the broken curve). Tsunami height was evaluated along water depth of 100 m (blue line on the map)

tsunami height estimation based on M_{BA} for a event similar to the 2006 Java earthquake. For that case, tsunami waring upgrade after the first tsunami warning based on a moment tensor estimation and off-shore tsunami gauge data would be important to mitigate tsunami disaster.

A uniform-slip fault model is often used for the tsunami height estimation in tsunami warning systems. We calculated tsunami height from a fault model with a uniform slip. A fault of length 71 km, width 35 km, and slip 2.1 m (M_w 7.3) was assumed following a uniform-slip fault model used by Nakata et al. (2019). Strike N188°E, dip 45°, rake 90°, top depth 2.4 km, and a fault corner location at 38.5°N, 143.8°E were used as fault parameters. The result of the calculation is show in Fig. 10 with those for the finite fault models. The top tsunami height of the uniform-slip fault model was about half of that for the finite fault model with the same moment magnitude. Although peak crustal deformation of the uniform-slip fault model was larger than that of the finite fault model of M_w 7.7, the resultant tsunami height was significantly smaller for the uniform-slip fault model. This tsunami height difference come from the crustal deformation distribution difference between the finite fault model and the uniform-slip fault model. Such difference should be taken into account as a safety factor of tsunami warning for events near the trench axis.

Time required for magnitude estimation

The time required for magnitude estimation is important for early tsunami warning. Comparison of M_{BA} with the time elapsed since the origin time for the fault models shown in Fig. 8 (Fig. 11) shows that the final magnitudes of the five events were reached within about 4 min, and some of them closely approached their final values within 3 min. Variations in the estimated duration with elapsed are also shown in Fig. 11. Because the assumed source duration greatly affects the amplitude distribution (Fig. 6), M_{BA} is greatly dependent on the estimated duration; thus the time needed to estimate the duration controls the time needed to estimate M_{BA}. To obtain the values shown in Table 2, the period ratio between the lower and upper passband was set at $10^{0.6}$. When a value of $10^{0.2}$ was used as the ratio between the lower and upper passband limits, we obtained M_{BA} values closer to M_w than those in the table, but 6–8 min were required for the magnitude estimation.

The estimated durations, which ranged from 20 to 50 s (Fig. 11), were much shorter than the source durations

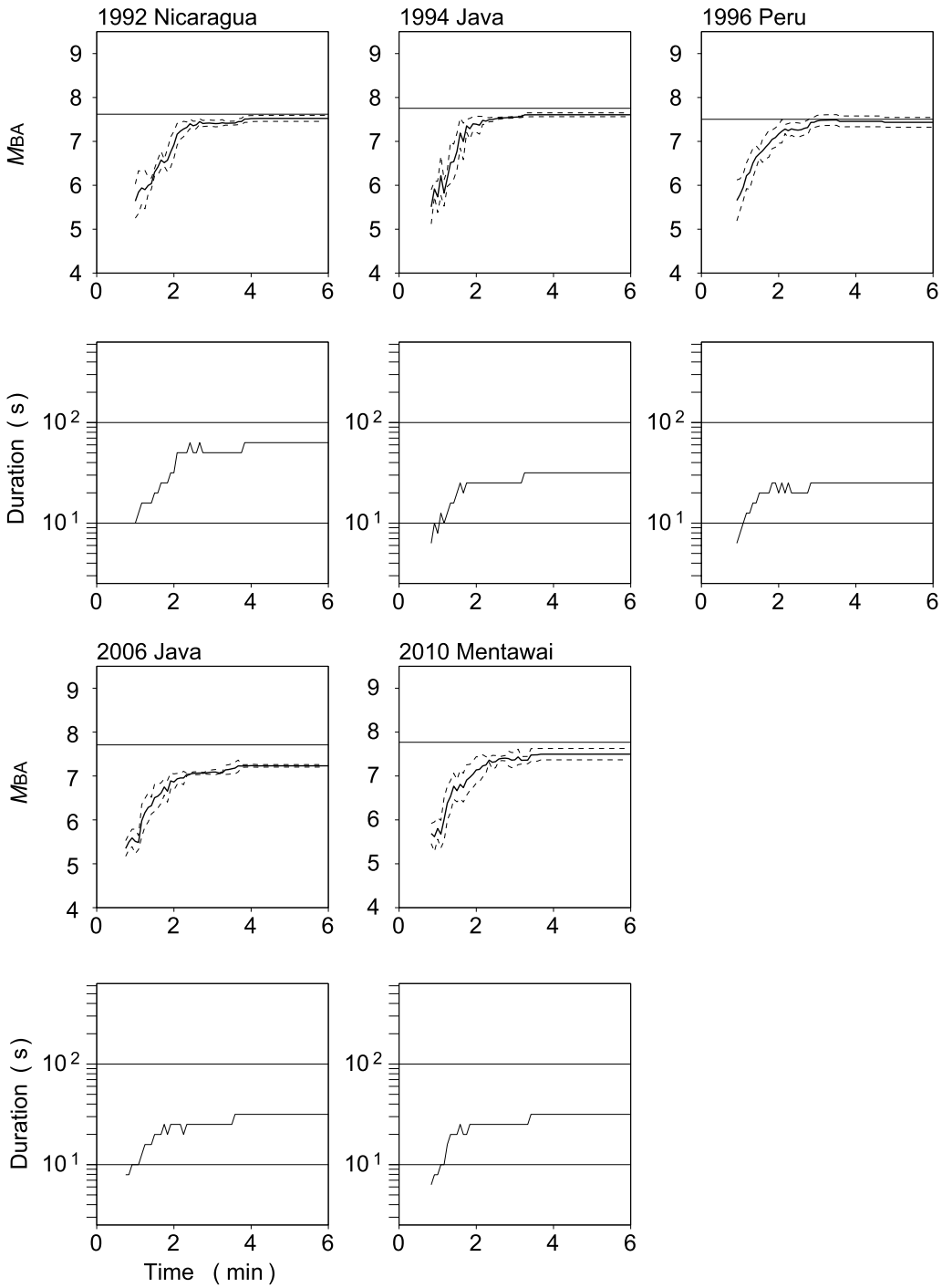

Fig. 11 Variations of the estimated magnitude (M_{BA}) (upper graph) and duration (lower graph) in relation to elapsed time from the origin for simulated data of five tsunami earthquakes (see Fig. 8). On the magnitude graphs, the horizontal solid line indicates M_w, and dashed lines show ± standard deviation of the estimated station magnitudes

indicated by the source time function (Fig. 8), because the estimated durations relate the characteristic period of the seismic waves at the observation sites rather than the actual source duration.

For the 1992 Nicaragua earthquake, we also compared the station number limit with the time required to approach the final M_{BA} and $M_{BA} - M_w$.

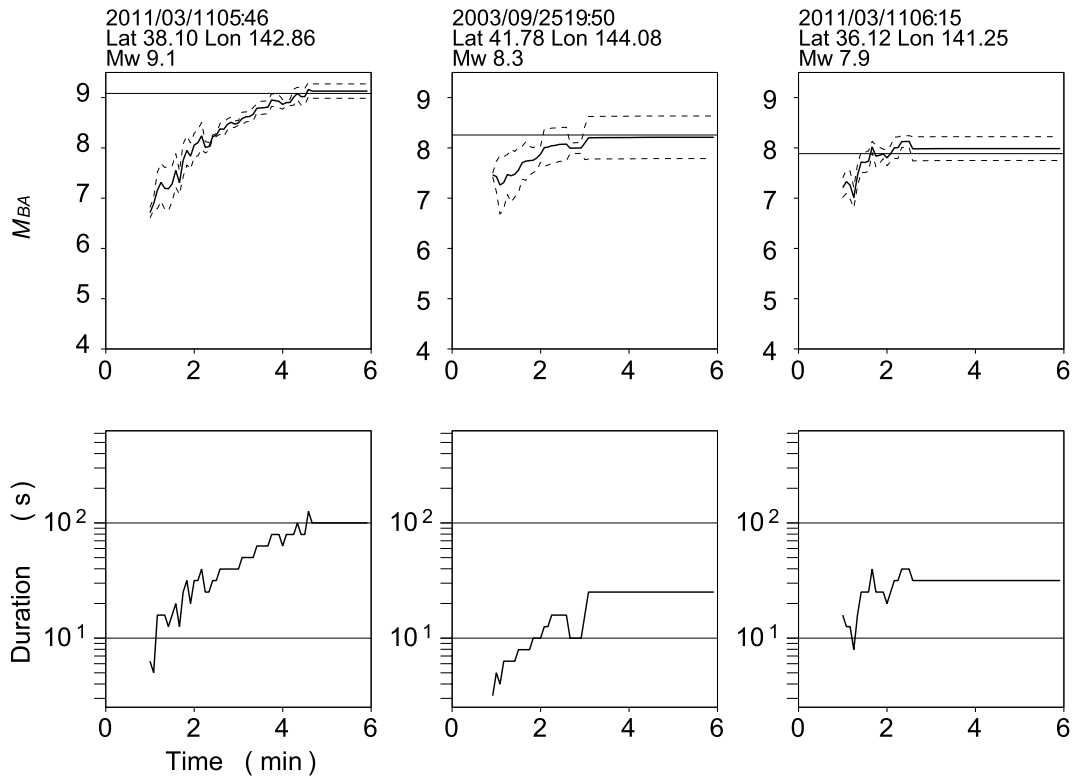

Fig. 12 Variations of the magnitude (M_{BA}) (upper graph) and duration (lower graph) estimated from observed data in relation to elapsed time from the origin for three large earthquakes around the Japanese Islands (the 2011 Tohoku earthquake M_w 9.1; the 2003 Tokachi-oki earthquake M_w 8.3; the largest aftershock of the 2011 Tohoku earthquake M_w 7.9). On the magnitude graphs, the horizontal lines indicate M_w and dashed lines M_w ±standard deviation of estimated station magnitudes

Although the time was reduced when fewer stations were used, the time reduction was negligible when the station number limit was set to less than under about 10. When only a small number of station were used, there were intervals during which estimation of M_{BA} failed. This result indicated the station number limit of 10 was appropriate from the perspective of magnitude estimation time.

Figure 12 shows variations of M_{BA} and the estimated durations obtained with observed data for three large earthquakes around the Japanese Islands. In the case of the 2011 Tohoku earthquake, M_{BA} approached the final value within an elapsed time of about 4 min, and in the case of the other events, M_{BA} approached the final value about 2 min. The long rupture duration (> 150 s; Yoshida et al. 2011) of the 2011 event seems to have prevented the magnitude from being estimated within 3 min. We also applied the M_{BA} method to events around the Kuril Islands and Taiwan, where few events have adequate azimuthal coverage of seismic stations, but we did not succeed in obtaining M_{BA} for many of these events because it was not possible to estimate dominant duration.

Conclusions

We developed a rapid magnitude estimation method for tsunami earthquakes based on the amplitude distribution of multi-bandpass-filtered records. We expect this method to be used soon after event detection but before seismic moment estimation. The multiband amplitude distribution was greatly affected by the source duration, which was estimated by comparison with synthetic records for various assumed source durations. The magnitude was estimated from the ratio of observed amplitudes to synthetic ones. Simulations with finite fault models demonstrated the effectiveness of this method for past tsunami earthquakes. Application to observed data also showed proper magnitude estimation for the 2010 Mentawai earthquake, a typical tsunami earthquakes. The intended use of this method is the issuance of the first tsunami warnings soon after event detection. By using the developed method, we were able to estimate the magnitudes of great earthquakes, including the 2011 Tohoku earthquake, within about 4 min.

Abbreviations
BB: Broadband seismometer; IRIS: Incorporated Research Institutions for Seismology; GNSS: Global Navigation Satellite System; NIED: The National Research Institute for Earth Science and Disaster Resilience; VSM: Velocity-type strong-motion seismometer.

Acknowledgements
We used seismic records archived by the National Research Institute for Earth Science and Disaster Resilience (NIED) and Incorporated Research Institutions for Seismology (IRIS) and data from the Global CMT Catalog of Columbia University. The Seismological Bulletin of Japan is published by the Japan Meteorological Agency with the cooperation of the Ministry of Education, Culture, Sports, Science and Technology of Japan based on data from NIED, Hokkaido University, Hirosaki University, Tohoku University, The University of Tokyo, Nagoya University, Kyoto University, Kochi University, Kyushu University, Kagoshima University, the National Institute of Advanced Industrial Science and Technology, the Geospatial Information Authority of Japan, the Japan Agency for Marine-Earth Science and Technology, the Association for the Development of Earthquake Prediction, the Incorporated Research Institutes for Seismology, the Japan Meteorological Agency, and the governments of Aomori Prefecture, the Tokyo Metropolitan Government, Shizuoka Prefecture, and Kanagawa Prefecture,. We used seismic record synthesis programs developed by Takeo (1985) and the tsunami simulation code JAGURS developed by Baba et al. (2017). We are greatly appreciate thoughtful comments from the two anonymous reviewers.

Open Access
This article is distributed under the terms of the Creative Commons Attribution 4.0 International License (http://creativecommons.org/licenses/by/4.0/), which permits unrestricted use, distribution, and reproduction in any medium, provided you give appropriate credit to the original author(s) and the source, provide a link to the Creative Commons license, and indicate if changes were made.

Authors' contributions
AK proposed the estimation methods and contributed to the data analyses, the synthetic record analyses, and manuscript preparation. MT contributed to the observed data analyses and preliminary manuscript. TN contributed to the synthetic record analyses. All authors read and approved the final manuscript.

Funding
This research was conducted with support from the Japan Meteorological Agency.

Availability of data and materials
The seismic data analyzed in this study are available at the National Research Institute for Earth Science and Disaster Resilience (NIED) F-net repository, http://www.fnet.bosai.go.jp/top.php, and the Incorporated Research Institutions for Seismology (IRIS) repository, https://ds.iris.edu/wilber3/find_event. The Global CMT catalog is available from the Global Centroid-Moment-Tensor Project repository, https://www.globalcmt.org/CMTsearch.html. The Seismological Bulletin of Japan is available from the Japan Meteorological Agency repository, https://www.data.jma.go.jp/svd/eqev/data/bulletin/index.html. Topographic data used for tsunami simulation is available from the Association for Promotion of Infrastructure Geospatial Information Distribution repository, https://www.geospatial.jp/ckan/dataset.

Declarations

Competing interests
The authors declare that they have no competing interests.

Authors' information
Affiliation of one of authors (AK) was changed from Meteorological Research Institute to University of Toyama (akatsuma@sus.u-toyama.ac.jp) after the submission.

Received: 5 October 2020 Accepted: 2 March 2021
Published online: 17 March 2021

References

Abercrombie RE, Antolik M, Felzer K, Ekström G (2001) The 1994 Java tsunami earthquake: Slip over a subducting seamount. J Geophys Res 106:6595–6607. https://doi.org/10.1029/2000JB900403
Aki K, Richards PG (2002) Quantitative seismology, 2nd edn. W. H. Freeman and Company, New York
Ammon CJ, Kanamori H, Lay T, Velasco AA (2006) The 17 July 2006 Java tsunami earthquake. Geophys Res Lett 33:L24308. https://doi.org/10.1029/2006GL028005
Baba T, Allgeyer S, Hossen J, Cummins PR, Tsushima H, Imai K, Yamashita K, Kato T (2017) Accurate numerical simulation of the far-field tsunami caused by the 2011 Tohoku earthquake, including the effects of Boussinesq dispersion, seawater density stratification, elastic loading, and gravitational potential change. Ocean Modelling 111:46–54. https://doi.org/10.1016/j.ocemod.2017.01.002
Bilek SL, Lay T (2002) Tsunami earthquakes possibly widespread manifestations of frictional conditional stability. Geophys Res Lett 2002;29:18. https://doi.org/10.1029/2002GL015215
Disaster Management Council of Japan, Cabinet Office (2003) Topographic data. https://www.geospatial.jp/ckan/dataset. Accessed 23 Nov 2020
Dziewonski AM, Chou T-A, Woodhouse JH (1981) Determination of earthquake source parameters from waveform data for studies of global and regional seismicity. J Geophys Res 86:2825–2852. https://doi.org/10.1029/JB086iB04p02825
Ekström G, Nettles M, Dziewonski AM (2012) The global CMT project 2004–2010: centroid-moment tensors for 13,017 earthquakes. Phys Earth Planet In 200–201:1–9. https://doi.org/10.1016/j.pepi.2012.04.002
Fan W, Bassett D, Jiang J, Shearer PM, Ji C (2017) Rupture evolution of the 2006 Java tsunami earthquake and the possible role of splay faults. Tectonophysics 721:143–150. https://doi.org/10.1016/j.tecto.2017.10.003
Fukuyama E, Ishida M, Hori S, Sekiguchi S, Watada S (1996) Broadband seismic observation conducted under the FREESIA Project. Rep Natl Res Inst Earth Sci Disas Prev 57:23–31 (In Japanese with English abstract)
Hara T (2007) Magnitude determination using duration of high frequency energy radiation and displacement amplitude: application to tsunami earthquakes. Earth Planets Space 59:561–565. https://doi.org/10.1186/BF03352718
Heinrich P, Schindele F, Guibourg S, Ihmlé PF (1998) Modeling of the February 1996 Peruvian tsunami. Geophys Res Lett 25:2687–2690. https://doi.org/10.1029/98GL01780
Ihmlé PF, Gomez J-M, Heinrich P, Guibourg S (1998) The 1996 Peru tsunamigenic earthquake: broadband source process. Geophys Res Lett 25:2691–2694. https://doi.org/10.1029/98GL01987
Japan Meteorological Agency (2013) Improvement in tsunami warning (in Japanese). https://www.data.jma.go.jp/svd/eqev/data/tsunami/kaizen/index.html. Accessed 27 June 2019
Japan Meteorological Agency (2019) Seismological Bulletin of Japan, https://www.data.jma.go.jp/svd/eqev/data/bulletin/index.html Accessed 30 Jun 2019
Johnson JM, Satake K (1997) Estimation of seismic moment and slip distribution of the April 1, 1946, Aleutian tsunami earthquake June 1997. J Geophys Res 1021:11765–11774. https://doi.org/10.1029/97JB00274
Kanamori H (1972) Mechanism of tsunami earthquake. Phys Earth Planet In 6:346–359. https://doi.org/10.1016/0031-9201(72)90058-1
Kanamori H (1977) The energy release in great earthquakes. J Geophys Res 82:2981–2987. https://doi.org/10.1029/JB082i020p02981
Kanamori H, Kikuchi M (1993) The 1992 Nicaragua earthquake: a slow tsunami earthquake associated with subducted sediments. Nature 361:714–716. https://doi.org/10.1038/361714a0
Kanamori H, Rivera L (2008) Source inversion of W phase: speeding up seismic tsunami warning. Geophys J Int 175:222–238. https://doi.org/10.1111/j.1365-246X.2008.03887.x
Katsumata A (1993) Automatic designing of Bessel digital filters. Q J Seismol 56:17–34 (In Japanese)
Katsumata A (2004) Revision of the JMA displacement magnitude. Q J Seismol 67:1–10 (In Japanese with English abstract)
Katsumata A, Ueno H, Aoki S, Yoshida Y, Barrientos S (2013) Rapid magnitude determination from peak amplitudes at local stations. Earth Planets Space 65:843–853. https://doi.org/10.5047/eps.2013.03.006
Kawamoto S, Ohta Y, Hiyama Y, Todoriki M, Nishimura T, Furuya T, Sato Y, Yahagi T, Miyagawa K (2017) REGARD: A new GNSS-based real-time finite fault

modeling system for GEONET. J Geophys Res 122:1324–1349. https://doi.org/10.1002/2016JB013485
Lay T, Ammon CJ, Kanamori H, Yamazaki Y, Cheung KF, Hutko AR (2011) The 25 October 2010 Mentawai tsunami earthquake (M_w 7.8) and the tsunami hazard presented by shallow megathrust ruptures. Geophys Res Lett 38:L06302. https://doi.org/10.1029/2010GL046552
Nakata K, Hayashi Y, Tsushima H, Fujita K, Yoshida Y, Katsumata A (2019) Performance of uniform and heterogeneous slip distributions for the modeling of the November 2016 off Fukushima earthquake and tsunami, Japan. Earth Planets Space 71:30. https://doi.org/10.1186/s40623-019-1010-1
National Research Institute for Earth Science and Disaster Resilience (2019) F-net. http://www.fnet.bosai.go.jp/top.php. Accessed 5 Jul 2019
Newman AV, Hayes G, Wei Y, Convers J (2011) The 25 October 2010 Mentawai tsunami earthquake, from real-time discriminants, finite-fault rupture, and tsunami excitation. Geophys Res Lett 38:L05302. https://doi.org/10.1029/2010GL046498
Okada Y (1992) Internal deformation due to shear and tensile faults in a half-space. Bull Seism Soc Am 82:1018–1040
Okal EA, Synolakis CE (2004) Source discriminants for near-field tsunamis. Geophys J Int 158:899–912. https://doi.org/10.1111/j.1365-246X.2004.02347.x
Polet J, Kanamori H (2000) Shallow subduction zone earthquakes and their tsunamigenic potential. Geophys J Int 142:684–702. https://doi.org/10.1046/j.1365-246x.2000.00205.x
Polet J, Thio HK (2003) The 1994 Java Tsunami earthquake and its "Normal" aftershocks. Geophys Res Lett 30:1474. https://doi.org/10.1029/2002GL016806
Satake K (1994) Mechanism of the 1992 Nicaragua tsunami earthquake. Geophys Res Lett 21:2519–2522. https://doi.org/10.1029/94GL02338
Takeo M (1985) Near-field synthetic seismograms taking into account the effects of anelasticity -The effects of anelastic attenuation on seismograms caused by sedimentary layer-. Pap Meteorol Geophys 36:245–257 (In Japanese with English abstract)
Tanioka Y, Satake K (1996) Fault parameters of the 1896 Sanriku tsunami earthquake estimated from tsunami numerical modeling. Geophys Res Lett 23:1549–1552. https://doi.org/10.1029/96GL01479
Tanioka Y, Seno T (2001) Sediment effect on tsunami generation of the 1896 Sanriku tsunami earthquake. Geophys Res Lett 28:3389–3392
Tsuboi S, Abe K, Takano K, Yamanaka Y (1995) Rapid determination of M_W from broadband *P* waveforms. Bull Seism Soc Am 85:606–613
U. S. Geological Survey (2020) Earthquake Hazards Program. https://earthquake.usgs.gov/earthquakes/search/. Accessed 5 Jan 2020
Ueno H, Hatakeyama S, Aketagawa T, Funasaki J, Hamada N (2002) Improvement of hypocenter determination procedures in the Japan Meteorological Agency. Q J Seismol 65:123–134 (In Japanese with English abstract)
Usui Y, Yamauchi T (2013) Automatic W phase inversion analysis using broadband seismometer in JMA. Q J Seismol 77:55–62 (In Japanese)
Yoshida Y, Ueno H, Muto D, Aoki S (2011) Source process of the 2011 off the Pacific coast of Tohoku Earthquake with the combination of teleseismic and strong motion data. Earth Planets Space 63:565–569. https://doi.org/10.5047/eps.2011.05.011
Zhu L (2003) Recovering permanent displacements from seismic records of the June 9, 1994 Bolivia deep earthquake. Geophys Res Lett 30:1740. https://doi.org/10.1029/2003GL017302

Publisher's Note

Springer Nature remains neutral with regard to jurisdictional claims in published maps and institutional affiliations.

Submit your manuscript to a SpringerOpen journal and benefit from:

- ► Convenient online submission
- ► Rigorous peer review
- ► Open access: articles freely available online
- ► High visibility within the field
- ► Retaining the copyright to your article

Submit your next manuscript at ► springeropen.com